

# Towards a Dynamical Collision Model of Highly Porous Dust Aggregates

Carsten Güttler<sup>\*</sup>, Maya Krause<sup>\*</sup>, Ralf Geretshauer<sup>†</sup>, Roland Speith<sup>†</sup> and Jürgen Blum<sup>\*</sup>

<sup>\*</sup>*Institut für Geophysik und extraterrestrische Physik, TU Braunschweig, Germany*

<sup>†</sup>*Institut für Astronomie und Astrophysik, Universität Tübingen, Germany*

**Abstract.** In the recent years we have performed various experiments on the collision dynamics of highly porous dust aggregates and although we now have a comprehensive picture of the micromechanics of those aggregates, the macroscopic understanding is still lacking. We are therefore developing a mechanical model to describe dust aggregate collisions with macroscopic parameters like tensile strength, compressive strength and shear strength. For one well defined dust sample material, the tensile and compressive strength were measured in a static experiment and implemented in a Smoothed Particle Hydrodynamics (SPH) code. A laboratory experiment was designed to compare the laboratory results with the results of the SPH simulation. In this experiment, a mm-sized glass bead is dropped into a cm-sized dust aggregate with the previously measured strength parameters. We determine the deceleration of the glass bead by high-speed imaging and the compression of the dust aggregate by x-ray micro-tomography. The measured penetration depth, stopping time and compaction under the glass bead are utilized to calibrate and test the SPH code. We find that the statically measured compressive strength curve is only applicable if we adjust it to the dynamic situation with a “softness” parameter. After determining this parameter, the SPH code is capable of reproducing experimental results, which have not been used for the calibration before.

**Keywords:** dust collisions, cohesive powder, modelling, planet formation

**PACS:** 96.10.+i

## INTRODUCTION

Planets form from micrometer-sized dust grains, colliding at low velocities and sticking to each other due to attracting van-der-Waals forces [1]. From the interplay between laboratory experiments [2] and molecular dynamic simulations [3, 4] we have a good picture of the microphysics of those processes, but as aggregates grow larger (e.g. 1 mm), the understanding of the collision mechanics is severely lacking. For these sizes (and the corresponding velocities), collisions between equal sized aggregates rather lead to bouncing or fragmentation than to sticking.

Millimeter-sized aggregates – as precursors of planets – are expected to be highly porous, having a volume filling factor (the volume fraction of material) of only few percent up to few ten percent. This strongly cohesive material is comparable to millimeter-sized dust clumps present in conventional dry powders (e.g. cocoa, confectioners’ sugar) but probably being more porous. One well analyzed analog material are dust aggregates formed by the random ballistic deposition (RBD) method, experimentally introduced in Ref. [5]. These dust aggregates have a volume filling factor of  $\phi = 0.15$  (for monospheric dust) and are produced in our laboratory in macroscopic 2.5 cm samples. Using these dust samples, we performed various collision experiments to study the further growth and evolution of planetary bodies [e.g. 1, 6]. However, as experiments cannot be performed for any relevant set

of parameters (e.g. collisions of meter-sized bodies), a collision model is required to cover the wide parameter space occurring for protoplanetary dust-aggregate collisions, i.e. dust aggregate sizes of up to 1 km and collision velocities in the range of  $10^{-3} - 10^2 \text{ m s}^{-1}$ . The approach is therefore to measure macroscopic parameters of the laboratory dust samples and implement them in a numeric simulation of a dust aggregate collision, which is concurrently performed in a laboratory experiment. Comparing experiment and simulation and defining and determining the free parameters, yields a calibrated collision model to perform collision simulations with parameters unaccessible to laboratory experiments.

## SMOOTHED PARTICLE HYDRODYNAMICS FOR DUST COLLISIONS

For the simulation of dust aggregate collisions we use the Smoothed Particle Hydrodynamics (SPH) method with extensions for the treatment of solid and porous media. A comprehensive description of the meshless Lagrangian particle method SPH can for example be found in [7]. In this scheme the continuous solid objects are discretized into interacting mass packages (“particles”) carrying all relevant continuous quantities. Time evolution is com-

puted according to the Lagrangian equations of continuum mechanics:

$$\frac{d\rho}{dt} + \rho \sum_{\alpha=1}^D \frac{\partial v_{\alpha}}{\partial x_{\alpha}} = 0 \quad (1)$$

$$\frac{dv_{\alpha}}{dt} = \frac{1}{\rho} \sum_{\beta=1}^D \frac{\partial \sigma_{\alpha\beta}}{\partial x_{\beta}} \quad (2)$$

Here,  $\rho$  denotes the density,  $v$  the velocity,  $D$  the dimension and  $\sigma_{\alpha\beta}$  the stress tensor, defined as

$$\sigma_{\alpha\beta} = -p\delta_{\alpha\beta} + S_{\alpha\beta}. \quad (3)$$

It consists of a pressure part with pressure  $p$  and a shear part given by the traceless deviatoric stress tensor  $S_{\alpha\beta}$ . Its time evolution is modelled according to Ref. [8]. This set of equations is closed by a suitable equation of state and describes the elastic behavior of a solid body. Together with a suitable damage model, which we do not adopt, the authors of Ref. [8] have modelled collisions between brittle basaltic rocks using this scheme.

In contrast to this, we simulate the plastic behavior of porous bodies. Therefore we adopt a modified version of the porosity model by Sirono [9]. According to this approach, plasticity is modelled within the equation of state and porosity is given by  $1 - \rho/\rho_0$ , where  $\rho$  denotes the actual and  $\rho_0$  the bulk density of the material. The pressure is limited by the compressive strength  $\Sigma(\rho)$  as upper bound and the (negative) tensile strength  $T(\rho)$  as lower bound. In between, the solid body experiences elastic deformation, whereas outside this regime it is deformed plastically. Thus, the full equation of state reads

$$p(\rho) = \begin{cases} \Sigma(\rho) & \rho > \rho_c^+ \\ K(\rho'_0)(\rho/\rho'_0 - 1) & \rho_c^- \leq \rho \leq \rho_c^+ \\ T(\rho) & \rho < \rho_c^- \end{cases} \quad (4)$$

The quantity  $\rho'_0$  denotes the density of the material at zero external stress.  $\rho_c^+$  and  $\rho_c^-$  are limiting quantities, where the transition between the elastic and plastic regime for compression and tension, respectively, takes place. Once a limit is exceeded, the material leaves the elastic path where energy is conserved, and loses internal energy by following the paths of the compressive and tensile strength.

In a previous work, Sirono [9] adopted power laws from measurements with toner particles for  $\Sigma(\rho)$ ,  $T(\rho)$  and the bulk modulus  $K(\rho)$  in order to simulate porous ice, which is a crude extrapolation. For our approach, we used the material properties, measured for well defined RBD dust aggregates [5]. For the tensile strength we adopted the measurement of Ref. [5] who measured the tensile strength for porous ( $\phi = 0.15$ ) and compact ( $\phi = 0.54$ ) aggregates and found an agreement with a linear

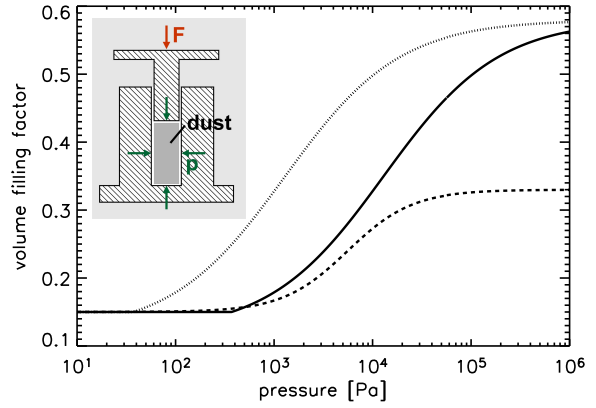


**FIGURE 1.** Compressive strength curve for unidirectional (dashed line), omnidirectional (solid line), and dynamic (dotted line) compression. The inset illustrates the setup for the omnidirectional compression measurement.

dependence between tensile strength and numbers of contact per cross-sectional area. This yields a tensile strength of

$$T(\phi) = -(10^{2.8+1.48\phi}) \text{ Pa}. \quad (5)$$

For the compressive strength we started with the compression curve  $\phi(\Sigma)$  measured in Ref. [5] (unidirectional, 1D compression) and also made a new compression measurement (omnidirectional, 3D, see inset in Fig. 1, [10]). Both compressive strength curves are displayed in Fig. 1. They resemble in shape and can be described by

$$\Sigma(\phi) = p_m \cdot \left( \frac{\phi_2 - \phi_1}{\phi_2 - \phi} - 1 \right)^{\Delta \cdot \ln 10}, \quad (6)$$

with four free parameters  $\phi_1$ ,  $\phi_2$ ,  $\Delta$ , and  $p_m$ . For unidirectional compression we found  $p_m = 5.6$  kPa,  $\phi_1 = 0.15$ ,  $\phi_2 = 0.33$ , and  $\Delta = 0.33$ , while for omnidirectional compression measurements performed in this work the parameters are identified as  $p_m = 13$  kPa,  $\phi_1 = 0.12$ ,  $\phi_2 = 0.58$ , and  $\Delta = 0.58$ . For unidirectional, static compression, the material can creep sideways, releasing pressure. As we did not observe this in the dynamic experiments (next section, Fig. 2), we expect omnidirectional compression, defining the parameters  $\phi_1$  and  $\phi_2$ . For low pressures,  $\Delta \cdot \ln 10$  is the slope of a power law found by divers authors [5, 11] and does not leave very much margin. Thus, we take  $p_m$  as the only free parameter with the most influence on material softness, shifting the compression curve towards lower pressures and determine  $p_m$  within the calibration procedure. As the the shear strength was not measured so far, we follow Sirono [9] and take  $Y = \sqrt{|\Sigma|T}$ .

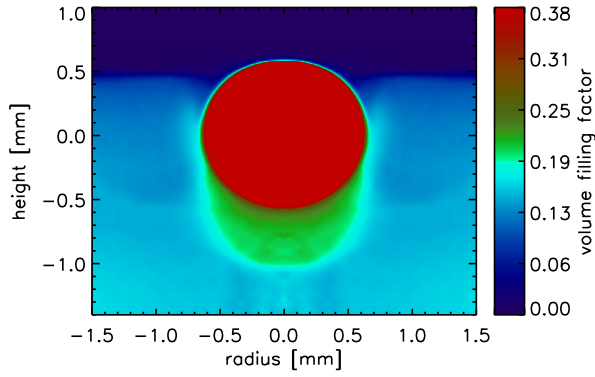


**FIGURE 2.** The density plot reveals the compaction of the dust sample under the glass bead (red, saturated) with a volume filling factor of 0.20 to 0.25 (green) in a well confined volume of approximately one sphere volume. The original dust material has a volume filling factor of 0.15 (light blue).

## CALIBRATION EXPERIMENT

In the experiments, a solid projectile was dropped into a 2.5 cm diameter, highly porous dust aggregate consisting of  $1.5 \mu\text{m}$   $\text{SiO}_2$  monomers (RBD dust aggregate from [5]). The experiments were performed in vacuum (0.1 mbar) such that gas effects did not play a role. The projectile was either a glass bead of 1 mm diameter or a cylindrical plastic tube with a 1 or 3 mm diameter epoxy droplet at the bottom (representing a 1 or 3 mm glass bead). The epoxy projectile had a mass corresponding to a glass bead and therefore was longer and could be observed for a penetration deeper than its diameter. For 15 experiments with elongated projectiles, the deceleration curve and, thus, the penetration depth and the stopping time were measured with a high-speed camera. The stopping time for one projectile diameter was found to be rather constant,  $(3.0 \pm 0.1)$  ms for 1 mm projectiles and  $(6.2 \pm 0.1)$  ms for 3 mm projectiles, while the penetration depth depended on the projectile size and the impact velocity (drop height). Details on the full deceleration curve can be found in [10]. The penetration depth could well be approximated by

$$D = \left( 8 \cdot 10^{-4} \frac{\text{m}^2 \text{s}}{\text{kg}} \right) \cdot \frac{mv}{A}, \quad (7)$$

where  $v$ ,  $m$ , and  $A = \pi R^2$  are the projectile velocity at the time of first contact, the projectile mass, and its maximum cross-sectional area (see also Fig. 4 in the next section). The stopping time and the relation for the penetration depth will be used for the calibration later on.

Two experiments with a 1 mm glass bead impacting with  $(0.8 \pm 0.1) \text{ m s}^{-1}$  were analyzed using an x-ray micro-tomograph (Micro-CT SkyScan 1074). In this method, the dust sample with the embedded glass bead

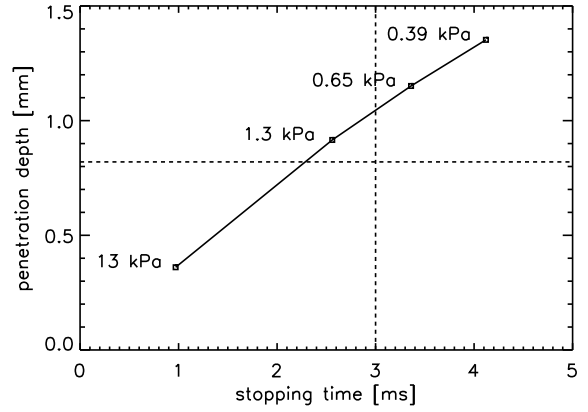


**FIGURE 3.** Varying the parameter  $p_m$  in the simulation changes the softness of the material and yields different penetration depths and stopping times. The best agreement with the experiments was found for  $p_m = 1.3$  kPa.

was positioned between an x-ray source and a detector and rotated stepwise. Based on the 400 resulting transmission images, a 3-dimensional density reconstruction was calculated using the SkyScan Cone-Beam Reconstruction Software. Assuming cylindrical symmetry in the axis of penetration, the density was averaged to one vertical section and displayed in the contour plot in Figure 2. The compaction of the dust is clearly visible in a confined volume under the sphere. The green color marking this volume denotes a volume filling factor of 0.20 to 0.25, while the material around this compaction zone is virtually unaffected with an original volume filling factor of  $\phi \approx 0.15$ . The distribution of compacted material will be used for the verification of the SPH code.

## CALIBRATION AND VERIFICATION OF THE SPH CODE

In the 2D SPH simulation, an infinite cylinder with 1.1 mm diameter ( $\rho = 2540 \text{ kg m}^{-3}$ ) impacts into a dust sample with a cross section of  $8 \times 5 \text{ mm}^2$  at a velocity of  $0.65 \text{ m s}^{-1}$ . For comparison with the 3D experiments a correction factor of  $\frac{8}{3\pi}$  for the penetration depth is required (see [10]). For the calibration we will use the penetration depth, which has to be 0.82 mm (Eq. 7 and correction factor), the stopping time of 3 ms, and the compaction under the glass bead from the x-ray experiments.

Using the shear strength formalism introduced by Sirono [9], e.g.  $Y = \sqrt{|\Sigma|T}$ , we have one free parameter with influence on the outcome of the simulations, i.e. the adjustment of the compressive strength curve for dynamic compression by the parameter  $p_m$  (see Eq. 6). A detailed study on the shear model can be found in [10].

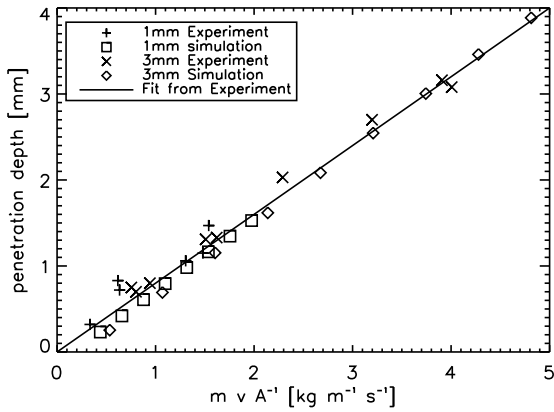


**FIGURE 4.** The penetration depth as a function of momentum per cross-sectional area can well be reproduced with the SPH code.

The parameter  $p_m$  defines the softness of the material and decreasing this parameter yields deeper penetrations. Figure 3 describes the calibration of this parameter. The horizontal line denotes the expected penetration depth from Eq. 7, while the vertical line represents a mean stopping time of 3 ms for 1 mm spheres. A value of  $p_m = 1.3$  kPa yields the best agreement with the experiments and thus we will use this value for further tests.

One test for the validation of the SPH code is the penetration depth relation for different sizes and different velocities, reproducing Eq. 7. The penetration depths of the experiments and the penetration depths of the simulations (with correction factor) are plotted in Fig. 4. For  $mvA^{-1} \gtrsim 1 \text{ kg m}^{-1} \text{ s}^{-1}$  experiment and simulation are in very good agreement and the SPH code succeeds in the scaling of radius and velocity.

A second validation test is the comparison of the compressed volume with the results of the x-ray measurement (Fig. 2). From the 3-dimensional density data, one can determine the volume fraction that is compressed to a given volume filling factor, which is plotted in Fig. 5. Approximately one sphere volume was compacted in total, while the values for  $\phi \lesssim 0.2$  represent the original material being distributed around the mean filling factor of 0.15. Also for this test, we find a good agreement between experiment and simulation.

## CONCLUSION

We have developed an SPH code for the description of collisional interaction between high-porosity dust aggregates. The code was calibrated by static and dynamic laboratory experiments using macroscopic RBD aggregates with an uncompressed filling factor of  $\phi = 0.15$ . The cal-

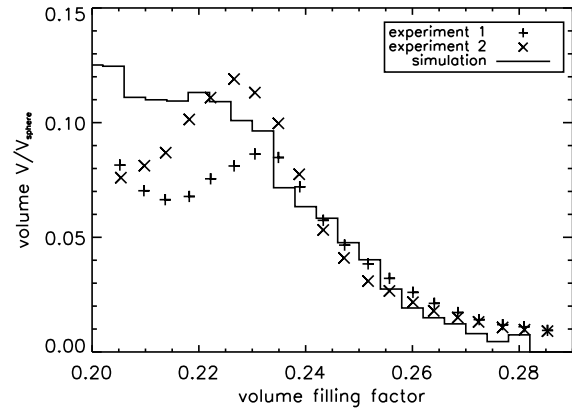


**FIGURE 5.** Experimental results (symbols) and simulation (solid line) of the compressed volume.

ibrated SPH code correctly predicts the size and velocity dependence of the penetration depth for an impacting solid projectile as well as the compressed volume.

## ACKNOWLEDGMENTS

We thank M.-B. Kallenrode and the University of Osnaabrück for providing access to the XRT setup. Simulations were performed on clusters of the computing center (ZDV) of the University of Tübingen. This project is funded by the Deutsche Forschungsgemeinschaft within the Forschergruppe 759 “The Formation of Planets: The Critical First Growth Phase” under grants Bl 298/7-1, Bl 298/8-1, and Kl 650/8-1.

## REFERENCES

1. J. Blum, and G. Wurm, *Annual Review of Astronomy and Astrophysics* **46**, 21–56 (2008).
2. J. Blum, and G. Wurm, *Icarus* **143**, 138–146 (2000).
3. D. Paszun, and C. Dominik, *Astronomy and Astrophysics* **484**, 859–868 (2008), 0802.1832.
4. C. Dominik, and A. G. G. M. Tielens, *The Astrophysical Journal* **480**, 647 (1997).
5. J. Blum, and R. Schräpler, *Physical Review Letters* **93**, 115503 (2004).
6. D. Langkowski, J. Teiser, and J. Blum, *The Astrophysical Journal* **675**, 764–776 (2008).
7. J. J. Monaghan, *Reports of Progress in Physics* **68**, 1703–1759 (2005).
8. W. Benz, and E. Asphaug, *Icarus* **107**, 98 (1994).
9. S.-I. Sirono, *Icarus* **167**, 431–452 (2004).
10. C. Güttler, M. Krause, R. Geretshäuser, R. Speith, and J. Blum, *The Physics of Protoplanetary Dust Agglomerates. IV. Towards a Dynamical Collision Model* (2009), in prep.

11. J. M. Valverde, M. A. S. Quintanilla, and A. Castellanos,  
*Physical Review Letters* **92**, 258303 (2004).